

1 **Calibration methods for laser ablation Rb–Sr geochronology:**
2 **comparisons and recommendation based on NIST glass and**
3 **natural reference materials**

4 Stijn Glorie^{1*}, Sarah E. Gilbert², Martin Hand¹, Jarred C. Lloyd¹

5 ¹ *Department of Earth Sciences, University of Adelaide, SA 5005, Australia.*

6 ² *Adelaide Microscopy, University of Adelaide, SA 5005, Australia.*

7
8 *Correspondence to: Stijn Glorie (stijn.glorie@adelaide.edu.au)*

9
10 **Abstract**

11 In-situ Rb–Sr geochronology using LA-ICP-MS/MS technology allows rapid dating of K-rich
12 minerals such as micas (e.g. biotite, muscovite, phlogopite) and K-feldspar. While many studies
13 have demonstrated the ability of the method, analytical protocols vary significantly and to date no
14 studies have provided an in-depth comparison and synthesis in terms of precision and accuracy.
15 Here we compare four calibration protocols based on commonly used reference materials for Rb–
16 Sr dating. We demonstrate that downhole fractionation trends (DHF) for natural biotite, K-feldspar
17 and phlogopite contrast with that for the commonly used Mica-Mg nano-powder reference
18 material. Consequently, Rb–Sr dates calibrated to Mica-Mg can be up to 5% inaccurate and the
19 degree of inaccuracy appears to be unsystematic between analytical sessions. Calibrating to Mica-
20 Mg also introduces excess uncertainty that can be avoided with a more consistent primary
21 calibration material. We propose a calibration approach involving (1) NIST-610 glass as the

22 primary reference material (PRM) for normalization and drift correction and (2) a natural mineral
23 with similar DHF characteristics to the analysed samples as matrix correction RM (MCRM) to
24 correct the Rb/Sr ratio for matrix-induced offsets. In this work, MDC phlogopite (the source
25 mineral for Mica-Mg nano-powder) was used as the MCRM, consistently producing accurate Rb–
26 Sr dates for a series of natural biotites and K-feldspars with well-characterized expected ages.
27 However, biotite from the Banalasta Adamellite, Taratap Granodiorite and Entire Creek pegmatite
28 are also suitable RMs for Rb/Sr ratio calibration purposes with consistently <1.5% fully
29 propagated uncertainties in our methodological approach. Until calibration using isochronous
30 natural standards as the primary RM becomes possible in data-reduction software, the two-step
31 calibration approach described here is recommended.

32

33 **Keywords:** reaction-cell ICP-MS; in-situ geochronology; Rb–Sr reference materials; calibration
34 standards

35

36 **1. Introduction**

37 Rubidium-Strontium (Rb–Sr) geochronology using laser ablation – inductively coupled plasma –
38 tandem mass spectrometry (LA-ICP-MS/MS) has become a popular method to constrain the
39 formation or cooling age of potassium-bearing minerals (Gorojovsky and Alard, 2020; Hogmalm
40 et al., 2017; Jegal et al., 2022; Kirkland et al., 2023; Larson et al., 2023; Laureijs et al., 2021; Li
41 et al., 2020; Liebmann et al., 2022; Olierook et al., 2020; Redaa et al., 2021; Rosel and Zack, 2022;
42 Sengun et al., 2019; Tillberg et al., 2021; Tillberg et al., 2020; Wang et al., 2022; Zack and
43 Hogmalm, 2016). In contrast to traditional Rb–Sr dating involving column-chemistry in

44 specialized laboratories, the laser-ablation method allows rapid acquisition of Rb–Sr dates directly
45 from thin sections or rock blocks with minimal sample preparation. The method involves the use
46 of an ICP-MS/MS, equipped with a reaction cell where isobaric isotopes can be chemically
47 separated due to their significant differences in reactivity with an introduced reaction gas (Balcaen
48 et al., 2015 and references therein). Applied to Rb–Sr geochronology, CH₃F, SF₆, O₂ and N₂O
49 have been used as reaction gasses (e.g. Hogmalm et al., 2017; Moens et al., 2001; Zack and
50 Hogmalm, 2016), with the latter being the most widely used for quadrupole ICP-MS/MS due to
51 its high reactivity. However, published analytical methodologies for LA-ICP-MS/MS Rb–Sr
52 dating vary significantly beyond the applied reaction gas (Table 1). Reported laser conditions
53 (fluence and repetition rate) are largely laser-wavelength dependent with common conditions
54 being either $\sim 5 - 7 \text{ J.cm}^{-2} / 10 \text{ Hz}$ for 213nm lasers, especially during initial development work
55 (e.g. Hogmalm et al., 2017; Laureijs et al., 2021; Rosel and Zack, 2022; Sengun et al., 2019;
56 Tillberg et al., 2020; Zack and Hogmalm, 2016) or $\sim 2 - 4 \text{ J.cm}^{-2} / 5 \text{ Hz}$ for 193nm lasers (e.g.
57 Kirkland et al., 2023; Larson et al., 2023; Li et al., 2020; Liebmann et al., 2022; Olierook et al.,
58 2020; Redaa et al., 2021). The applied calibration protocols for mass discrimination and elemental
59 fractionation, however, vary more significantly.

60 We define three types of reference materials (RM) in this manuscript:

61 (1) The Primary RM (PRM) has a homogenous isotopic composition and is used for
62 normalisation and drift correction;

63 (2) The matrix correction RM (MCRM) has a heterogenous isotopic composition but well-
64 known age and is used to correct the Rb/Sr ratio for systematic matrix-induced off-sets
65 between the PRM and mineral samples.

66 (3) The secondary RM (SRM) has a well-known age and a similar composition to the analysed
67 samples and is used to verify the accuracy of the calibration protocol.

68 Most published work uses a glass reference material as PRM, with NIST-610 being most popular
69 to correct for drift and calibrate the Sr isotopic ratios. Rb/Sr ratios are most commonly calibrated
70 against Mica-Mg, a phlogopite prepared as a pressed nano-powder pellet, regardless of the
71 analysed mineral (micas in most published work). However, the approach varies, with some
72 methods directly calibrating to Mica-Mg as the PRM (e.g. Gorojovsky and Alard, 2020; Hogmalm
73 et al., 2017; Li et al., 2020; Redaa et al., 2021; Rosel and Zack, 2022; Sengun et al., 2019; Wang
74 et al., 2022) and others using NIST-610 as the PRM followed by a correction for matrix-dependent
75 fractionation against Mica-Mg as MCRM (e.g. Liebmann et al., 2022; Olierook et al., 2020).
76 Secondary RMs, used to verify the accuracy of obtained dates, are either glass reference materials
77 (e.g. Larson et al., 2023; Laureijs et al., 2021; Rosel and Zack, 2022) or in-house natural materials
78 such as the La Posta biotite (Zack and Hogmalm, 2016), the MDC phlogopite (Redaa et al., 2021),
79 or the CK001 biotite (Olierook et al., 2020).

80 In addition, laser-induced down-hole fractionation (DHF) can occur during ablation and aerosol
81 condensation processes and is most apparent when ratioing elements with contrasting volatilities
82 (e.g. Jackson and Günther, 2003; Košler et al., 2005; Longerich et al., 1996). Elemental Sr is more
83 refractory than the volatile Rb and hence has a high potential to fractionate during laser ablation
84 (Zack and Hogmalm, 2016). A small number of studies have directly compared different
85 calibration approaches and have described differences in Rb–Sr DHF behaviour between
86 commonly used reference materials (e.g. Redaa et al., 2021; Wang et al., 2022). However,
87 systematic comparisons between data reduction protocols, tested with natural materials, are limited
88 in the current literature. Here, we compare four different calibration approaches for a series of

89 natural biotite and K-feldspar samples. The samples were taken from quickly cooled igneous rocks,
90 eliminating potential diffusion-related issues when comparing dates of different minerals. Hence,
91 the well-constrained igneous crystallization ages are the expected reference ages for the analysed
92 samples and one of the biotite samples has previously been dated by the Rb–Sr ID-TIMS method.
93 The calibration approaches we compare are:

94 (A) NIST-610 as the PRM for both $^{87}\text{Rb}/^{87}\text{Sr}$ and $^{87}\text{Sr}/^{86}\text{Sr}$ ratios plus MDC phlogopite as MCRM;

95 (B) NIST-610 as the PRM for both $^{87}\text{Rb}/^{87}\text{Sr}$ and $^{87}\text{Sr}/^{86}\text{Sr}$ ratios plus Mica-Mg pressed pellet as
96 MCRM;

97 (C) Mica-Mg as the PRM for $^{87}\text{Rb}/^{87}\text{Sr}$ ratios and NIST-610 as the PRM for $^{87}\text{Sr}/^{86}\text{Sr}$ ratios;

98 (D) Mica-Mg as the PRM for both $^{87}\text{Rb}/^{87}\text{Sr}$ and $^{87}\text{Sr}/^{86}\text{Sr}$ ratios

99 We discuss the differences between these approaches in terms of accuracy and precision, and
100 highlight the importance of monitoring and correcting down-hole fractionation with appropriate
101 reference materials.

102

103 **2. Sample descriptions**

104 **2.1. MDC phlogopite and Mica-Mg nano powder**

105 Mica-Mg nano-powder is used as a reference material for Rb–Sr dating. It consists of crushed
106 phlogopite from Bekily (Madagascar) with a high Rb ($1300 \pm 40 \mu\text{g}\cdot\text{g}^{-1}$) and low Sr ($27 \pm 3 \mu\text{g}\cdot\text{g}^{-1}$)
107 concentration (Redaa et al., 2023 and references therein). MDC is natural phlogopite, which was
108 sourced from the same locality as Mica-Mg (Redaa et al., 2021). The reference age for both
109 materials is $519.4 \pm 6.5 \text{ Ma}$ and the initial $^{87}\text{Sr}/^{86}\text{Sr}$ ratio is 0.72607 ± 0.0007 (2SE uncertainties),

110 constrained from a diopside (low-Rb mineral) that occurs in the same location (Hogmalm et al.,
111 2017). However, for Mica-Mg some pellet to pellet variation in both Rb/Sr and Sr/Sr ratios has
112 been observed (Jegal et al., 2022; Redaa et al., 2023).

113 **2.2. Entire Creek pegmatite**

114 The Entire Creek sample was taken from a deformed pegmatite in the Harts Range meta-igneous
115 complex of central Australia, in the same location as described by Mortimer et al. (1987). The
116 pegmatite cross-cuts folded and foliated amphibolites, is composed of coarse-grained quartz,
117 plagioclase, alkali feldspar and biotite, with the latter defining a strong axial-plane foliation to
118 folds outlined by the pegmatite. Biotite and whole-rock Rb/Sr and Sr/Sr isotope ratios, obtained
119 by ID-TIMS at the University of Adelaide, are reported in Mortimer et al. (1987) and define a 7-
120 point (3 biotite and 4 whole rock analyses) isochron age of $312.1 \pm 1.8 / 5.1$ Ma (95% confidence
121 uncertainties, without / with overdispersion), recalculated in IsoplotR (Vermeesch, 2018), using
122 the Villa et al. (2015) Rb–Sr decay constant of $1.3972 \pm 0.0045 \times 10^{-11} \text{ a}^{-1}$ (Appendix 1).

123 **2.3. Banalasta Adamellite (Bundarra Suite)**

124 The S-type Banalasta Adamellite forms the southern end the Bundarra Batholith in the Southern
125 New England Orogen in eastern Australia (e.g. Flood and Shaw, 1975; Jeon et al., 2012;
126 Rosenbaum et al., 2012; Shaw and Flood, 1981). The Bundarra Batholith is an elongate north-
127 south trending magmatic suite, spanning approximately 200 km. The Banalasta Adamellite is
128 approximately 40 km in diameter and has sharp contacts with surrounding metasediments with a
129 contact metamorphic aureole characterised by fine-grained cordierite-bearing assemblage at the
130 pluton margin grading out to regional prehnite-pumpellyite metagreywacke assemblages over a
131 distance of approximately 3 km (Flood and Shaw, 1977). Internally the granite is massive, coarse-

132 grained granitoid containing approximately equal proportions of K-feldspar and plagioclase,
133 together with accessory apatite, zircon and monazite. Biotite predominantly occurs in multi-grain
134 clots together with quartz, plagioclase, magnetite, zircon and apatite. In rare cases they contain
135 relic garnet, suggesting they formed from hydration of garnet entrained from the granitic source
136 region.

137 Melt-precipitated zircon from the Banalasta Adamellite gives zircon U-Pb ages of 286.2 ± 2.2 Ma
138 (Black, 2007), 289.2 ± 1.7 Ma (Jeon et al., 2012) and 282 ± 4 Ma (Phillips et al., 2011). Whole
139 rock Rb–Sr data from the Bundarra Suite gives an age of 285 ± 15 Ma ($n = 6/7$, MSWD = 0.4).
140 When additional feldspar Rb–Sr data are included in the isochron, the isochron age is 283 ± 10 Ma
141 ($n = 9/10$, MSWD = 0.24) (Appendix 2). Both isochron dates were recalculated using the data from
142 Flood and Shaw (1977) and the decay constant from Villa et al. (2015). Additionally, Hensel et al
143 (1995) reported a model whole rock Rb–Sr age of 287 ± 10 Ma for a group of 16 samples from the
144 Bundarra Suite. Overall, it is evident that Rb–Sr age data is similar to the ages of melt precipitated
145 zircon, consistent with the lack of evidence for extended fractional crystallisation (Jeon et al 2012).
146 The samples used in this study come from the same location as Black (2007) that has a granitic
147 zircon of 286.2 ± 2.2 Ma, as well as a second location approximately 800 meters away.

148

149 **2.4. Taratap Granodiorite**

150 The Taratap Granodiorite in the Delamerian Orogenic belt in southern Australia is classified as S-
151 type, calc-alkaline with a composition dominated by microcline megacrysts (c. 3–4 cm in length),
152 which define a NNE-trending magmatic fabric in a coarse-grained groundmass of plagioclase,
153 quartz, K-feldspar and biotite, with accessory zircon, apatite, and monazite. Low-temperature

154 alteration is evident in thin section by the presence of chlorite–muscovite–titanite and minor
155 allanite (Burt and Abbot, 1998). The sample was chosen for analysis because the timing of
156 emplacement is tightly constrained by a zircon U-Pb ID-TIMS age of 497.11 ± 0.56 Ma ($^{206}\text{Pb}/^{238}\text{U}$
157 weighted mean age, 95% confidence interval uncertainty, MSWD = 1.8, n = 6) and an apatite Lu-
158 Hf age of 497.1 ± 5.5 Ma (MSWD = 1.1, n = 38) (Glorie et al., 2023 and references therein).

159

160 **3. Analytical methods**

161 All Rb–Sr analyses were conducted at Adelaide Microscopy, University of Adelaide, using an
162 Agilent 8900x ICP-MS/MS, coupled to a RESolution-LR ArF excimer (193 nm) laser ablation
163 system. A squid mixing device (Laurin Technic) was used to smooth the pulsed laser signal
164 between the laser and the mass-spectrometer. The instrument parameters follow those reported in
165 Redaa et al. (2021), with ablation in a He atmosphere ($350 \text{ mL}\cdot\text{min}^{-1}$), mixed with Ar ($890 \text{ mL}\cdot\text{min}^{-1}$)
166 as the carrier gas and N_2 ($3.5 \text{ mL}\cdot\text{min}^{-1}$) added before the ICP torch to enhance the signal
167 sensitivity. N_2O ($0.37 \text{ mL}\cdot\text{min}^{-1}$) was used as the reaction gas to separate ^{87}Sr from ^{87}Rb . The ^{86}Sr
168 and ^{87}Sr isotopes were measured as their oxide reaction products (e.g. $^{87}\text{Sr}^{16}\text{O}$) with a mass shift
169 of 16 amu between the two quadrupole mass analysers (e.g. Q1 = 87 m/z, Q2 = 103 m/z). Despite
170 the high reaction efficiency of ^{87}Sr , residual unreacted Sr prevents direct measurement of ^{87}Rb .
171 Instead, ^{85}Rb was measured as a proxy for ^{87}Rb and calculated assuming natural isotopic
172 abundance. The samples and reference materials were ablated using a circular laser beam of 67
173 μm diameter, a fluence of $3.5 \text{ J}\cdot\text{cm}^{-2}$, and repetition rate of 5 Hz. Further details are presented in
174 Table 2. A total of three analytical sessions were conducted, with largely identical instrumental
175 parameters between the different sessions. The ICP-MS was tuned to a sensitivity which kept Rb

176 in pulse mode in Mica-Mg (the material with the highest Rb concentration), negating the
177 requirement for additional pulse-analogue (P/A) corrections.

178 For each analytical session, NIST-610, Mica-Mg and MDC were used as reference materials for
179 calibration purposes. All data was processed in LADR (Norris and Danyushevsky, 2018) using an
180 in-built data reduction algorithm that calculates error correlations (Pearson correlation coefficient)
181 from the raw isotopic ratios for each sweep in an analysis, in the same way as for U-Pb data
182 reduction. Isotope ratios were calculated by: (1) background subtraction, (2) correcting down-hole
183 fractionation (DHF) against the PRM, (3) averaging the DHF corrected ratios of each sweep in the
184 analysis, and then (4) normalising to the PRM to correct for matrix independent instrument mass
185 bias and drift. LADR applies a robust uncertainty propagation using the total uncertainty budget
186 of the measured quantified ratios. An example of an 'uncertainty tree', which can be queried for
187 every analysis, is given in Appendix 3. The reader is referred to the LADR software manual
188 (<https://norsci.com/?p=ladr-support>) for further details.

189 Normalisation of the measured Rb/Sr and Sr/Sr ratios was conducted with two different reference
190 materials (NIST-610 and Mica-Mg), following the four analytical protocols outlined above (A-D).
191 The reference $^{87}\text{Rb}/^{87}\text{Sr}$ and $^{86}\text{Sr}/^{87}\text{Sr}$ ratios used for Mica-Mg were 83.4 ± 1.0 and $0.53981 \pm$
192 0.00070 , respectively (Hogmalm et al., 2017). For NIST-610, the $^{87}\text{Rb}/^{87}\text{Sr}$ was calculated from
193 ppm data (GeoREM preferred values) as 3.28 ± 0.03 and for the $^{86}\text{Sr}/^{87}\text{Sr}$ ratio, the reference value
194 of 1.409048 ± 0.000036 was used (Woodhead and Hergt, 2001). For each normalization protocol,
195 DHF corrections of the $^{87}\text{Rb}/^{87}\text{Sr}$ ratios were applied based on the DHF behaviour of the applied
196 PRM. No DHF correction was applied to the $^{86}\text{Sr}/^{87}\text{Sr}$ ratios. Where NIST-610 was used as the
197 PRM, MDC phlogopite or Mica-Mg were used as MCRM to correct the $^{87}\text{Rb}/^{87}\text{Sr}$ ratios for matrix-

198 dependant fractionation (cfr. Roberts et al., 2017 for U/Pb ratios; Simpson et al., 2022 for Lu/Hf
199 ratios).

200 All mica samples (including biotite samples and MDC phlogopite) were ablated with the laser
201 ablating parallel to cleavage. The Bundarra and Taratap samples were analysed in thin section and
202 optical microscopy (birefringence) was used to only select ablation targets with upright ($\pm 10^\circ$)
203 cleavage. The coarse Entire Creek biotites were mounted as mica-books using a vice to prevent
204 air-gaps between individual mica sheets, with the ‘pages’ of the book mounted upright exposing
205 multiple cleavage planes perpendicular to the surface.

206 For each sample and reference material, inverse isochron Rb–Sr dates (Li and Vermeesch, 2021)
207 were calculated in IsoplotR (Vermeesch, 2018), based on the processed $^{87}\text{Rb}/^{87}\text{Sr}$ and $^{86}\text{Sr}/^{87}\text{Sr}$
208 ratios, their 2SE uncertainties, and the calculated error correlations. Reported inverse isochron
209 uncertainties are fully propagated 95% confidence intervals, including the uncertainty on the decay
210 constant and added uncertainty for overdispersion where required (calculated in IsoplotR). The
211 exceptions are the inverse isochron dates for MDC and Mica-Mg when used as MCRMs, which
212 are used to correct the Rb/Sr ratios after calibrating to NIST-610. For these cases the reported
213 uncertainties are 95% confidence uncertainties without external uncertainties (as the external
214 uncertainties would otherwise be applied twice to the isochron dates of the analysed samples).
215 Session-dependant correction factors (CF) were calculated from the measured $^{87}\text{Rb}/^{87}\text{Sr}$ ratio for
216 MDC and Mica-Mg (after drift corrections) and compared to the reference value (calculated from
217 the published age for both MDC and Mica-Mg of 519.4 ± 6.5 Ma; Högalm et al., 2017; Redaa
218 et al., 2021). These CF values (= measured ratio/expected ratio) were subsequently applied to each
219 unknown analysis when calibrated to either MDC or Mica-Mg. Finally, the uncertainties on the

220 MDC and Mica-Mg dates are propagated to the reported Rb–Sr isochron uncertainties for each
221 NIST-610 calibrated sample using the quadratic addition of the relative uncertainties.

222

223 **4. Results**

224 **4.1. Downhole fractionation trends**

225 In this section, we compare the downhole fractionation (DHF) trend of the $^{87}\text{Rb}/^{87}\text{Sr}$ ratio between
226 the analysed feldspars and micas and the reference materials (NIST-610 and Mica-Mg) (Fig. 1).
227 The obtained fractionation trends do not vary significantly between different sessions; however,
228 data from analytical session 3 is presented as it contains data for all analysed samples presented in
229 this paper. The DHF trends were calculated in LADR and individual scatter plots can be found in
230 Appendix 4. As shown, The DHF trends for the analysed biotite, phlogopite and K-feldspar
231 samples are internally consistent, showing $\sim 10\%$ increase in Rb/Sr ratio over the first 20 s of
232 ablation, followed by a flatter trend in the subsequent 20 s. NIST-610 shows a similar trend of
233 increasing Rb/Sr ratio with ablation time, however the amplitude of the DHF curve is more
234 subdued compared to the natural samples ($\sim 3.5\%$ increase in the first 20 s ablation). In contrast,
235 the DHF pattern for Mica-Mg shows an oscillating trend, increasing for the first ~ 10 s of ablation
236 and then dropping for the subsequent ~ 30 s of ablation (Fig. 1).

237

238 **4.2. Within-session reproducibility of $^{87}\text{Rb}/^{87}\text{Sr}$ and $^{86}\text{Sr}/^{87}\text{Sr}$ ratios**

239 Figure 2 shows the within-session variability (prior to drift correction) of the $^{87}\text{Rb}/^{87}\text{Sr}$ and
240 $^{86}\text{Sr}/^{87}\text{Sr}$ ratios for both PRMs NIST-610 and Mica-Mg in analytical session 3. The reference
241 materials are considered homogenous in both isotopic ratios, meaning that any variations are

242 purely due to differences in the ablation characteristics from spot to spot. As shown, the measured
243 $^{87}\text{Rb}/^{87}\text{Sr}$ ratios and $^{86}\text{Sr}/^{87}\text{Sr}$ ratios are significantly more consistent for NIST-610 compared to
244 Mica-Mg (both measured using the same analytical conditions and spot size). The maximum
245 within-session variability (=min-max range) in the $^{87}\text{Rb}/^{87}\text{Sr}$ ratio is < 3% for NIST-610, compared
246 to > 8% for Mica-Mg. The $^{86}\text{Sr}/^{87}\text{Sr}$ ratio is more consistent for both RMs, however, the uncertainty
247 on individual analyses is approximately 3× larger for Mica-Mg compared to NIST-610. ICP-MS
248 mass-bias drift is minimal for both isotope ratios in NIST-610, with only a slight increase in the
249 Rb/Sr ratio over the first 2-3 hours of analysis. As both Mica-Mg and NIST-610 were analysed
250 sequentially in the same analytical session, the apparent ‘drift’ in the Mica-Mg $^{86}\text{Sr}/^{87}\text{Sr}$ ratios are
251 due to variations in ablation rather than changes in the ICP-MS mass bias.

252 **4.3. Isochron Rb–Sr dates for natural K-feldspars and micas**

253 Inverse isochron plots and resulting Rb–Sr dates are presented for each analytical protocol in
254 Appendix 5. Summary plots are shown in Figure 3. The data-table with the input $^{87}\text{Rb}/^{87}\text{Sr}$ and
255 $^{86}\text{Sr}/^{87}\text{Sr}$ ratios is accessible from Figshare via the link in the data availability section. For the
256 Bundarra samples, the biotite isochrons are anchored to apatite Rb/Sr ratios, given that the apatites
257 commonly occur as inclusions within biotite. For the K-feldspars, the isochrons are anchored to
258 plagioclase, given that the analysed K-feldspars often show minor exsolution with plagioclase.
259 However, the choice of anchoring mineral gives no difference in the obtained biotite and K-
260 feldspar inverse isochron Rb/Sr dates. For the Taratap sample, isochron anchoring was conducted
261 to a combination of plagioclase and apatite in session 1, but only plagioclase in sessions 2 and 3,
262 given the limited occurrence of apatite in thin section. For the Entire Creek biotite sample,
263 anchoring was conducted to whole-rock $^{86}\text{Sr}/^{87}\text{Sr}$ ratios from Mortimer et al. (1987). The MDC

264 and Mica-Mg isochrons were anchored to an initial $^{86}\text{Sr}/^{87}\text{Sr}$ ratio of 1.3773 ± 0.0013 and
265 calibrated to the published age of 519.4 ± 6.5 Ma (Hogmalm et al., 2017; Redaa et al., 2021).

266 The summary of obtained inverse Rb–Sr dates is presented in Table 3. As shown, there is only
267 marginal variation in the absolute biotite dates between the three analytical protocols involving
268 Mica-Mg, either as the PRM for Rb/Sr ratios (protocols C & D) or as a MCRM (protocol B).
269 Hence, in order to evaluate the accuracy of the obtained Rb–Sr dates against the expected
270 references ages for each sample, we only compare the first two analytical protocols (NIST-610 as
271 the PRM and either: (A) MDC or (B) Mica-Mg as MCRM).

272 Figure 4 compares the obtained Rb–Sr inverse isochron dates to the expected ages for the three
273 samples, that were analysed over two or three analytical sessions. The uncertainties for the K-
274 feldspar dates are not shown as they are too large to be useful (due to the relatively low radiogenic
275 nature of typical K-feldspar versus micas), here we only compare the accuracy of the absolute
276 dates. As shown, analytical protocol (A) involving NIST-610 as PRM and MDC phlogopite as
277 MCRM consistently gives the most accurate Rb–Sr dates across all different analytical sessions.
278 For this analytical protocol, the Rb–Sr biotite dates for the Bundarra samples are 287.1 ± 2.4 Ma,
279 284.7 ± 3.0 Ma, 287.7 ± 2.3 Ma and 285.7 ± 2.6 Ma (between two samples over two analytical
280 sessions), which are in excellent agreement with the published zircon U-Pb age of 286.2 ± 2.2 Ma
281 (Black, 2007) from the same outcrop. The K-feldspar dates of 290 ± 14 Ma, 285 ± 15 Ma, 290 ± 37
282 Ma and 288 ± 37 Ma are in excellent agreement as well but are less useful to evaluate age
283 accuracies given their larger uncertainties. Similarly for the Taratap sample, the obtained biotite
284 Rb–Sr dates of 499.4 ± 3.6 Ma and 495.7 ± 4.0 Ma as well as the (imprecise) K-feldspar Rb–Sr
285 dates of 500 ± 30 Ma, 501 ± 50 Ma and 495 ± 35 Ma are in excellent agreement with the zircon
286 U-Pb ID-TIMS age of 497.1 ± 0.6 Ma as well as the apatite Lu-Hf age of 497.1 ± 5.5 Ma for the

287 same sample (Glorie et al., 2023). Hence, the combined dataset suggests that the biotite, K-feldspar
288 and zircons record the same (crystallization) age for both the Bundarra and Taratap samples. The
289 Entire Creek biotite gave consistent Rb–Sr dates of 310.7 ± 1.5 Ma and 311.6 ± 3.1 Ma, in excellent
290 agreement with the ID-TIMS age of $312.1 \pm 1.8 / 5.1$ Ma (95% confidence uncertainties, without
291 / with overdispersion), based on the Rb/Sr ratios in Mortimer et al. (1987), recalculated with the
292 Villa et al. (2015) Rb–Sr decay constant.

293 **5. Discussion**

294 **5.1. Downhole fractionation corrections**

295 Few previous studies have reported Rb–Sr DHF trends for a series of artificial reference materials
296 (i.e. glass standards and pressed pellets; Redaa et al., 2021; Wang et al., 2022). However, to the
297 best of our knowledge, DHF trends have not been evaluated for natural materials with the
298 exception of phlogopite MDC (Redaa et al., 2021). In our experiments, DHF is more pronounced
299 in natural micas and K-feldspar than observed for the NIST-610 glass and Mica-Mg pressed pellet,
300 when ablated under the same analytical conditions (Fig. 1). Comparatively, Mica-Mg appears least
301 appropriate to correct the analysed samples for DHF, given its systematically different DHF trend.
302 NIST-610 shows less DHF compared to the analysed micas and K-feldspars but its trend is more
303 systematic (similar shape with lower amplitudes). Thus, correcting for DHF against NIST-610
304 reduces the observed DHF for the analysed samples, while Mica-Mg significantly under-corrects
305 for DHF or accentuates it when applied to minerals. MDC biotite would be the most appropriate
306 choice for DHF correction as it behaves very similar to the analysed mica and K-feldspar samples.
307 However, as with most natural materials, MDC is not sufficiently homogenous in $^{87}\text{Rb}/^{87}\text{Sr}$ ratio
308 to be used as a PRM. While the shape or slope of DHF trends can vary depending on laser
309 conditions (spot size, frequency and fluence), it cannot be eliminated for elements with contrasting

310 volatilities such as Rb and Sr. However, based on the presented data, the use of NIST-610 is the
311 more appropriate reference material to correct for DHF and Mica-Mg would exacerbate instead of
312 reduce the effects of DHF.

313 If no DHF correction is applied, accurate data can only be achieved if exactly the same signal
314 interval is selected in both the RM and sample. If there is a residual DHF slope on the sample
315 Rb/Sr ratios that is different to the RM (e.g. crystalline material versus Mica-Mg), then selecting
316 a shorter signal interval can significantly bias Rb/Sr ratios and hence the apparent age.

317

318 **5.2. Mica-Mg vs NIST-610 and MDC as calibration standards**

319 **5.2.1. Uncertainty comparisons**

320 The contributions to the propagated uncertainties of individual analyses from the reference
321 materials (average signal precision and calibration curve misfit) are much larger when calibrating
322 to Mica-Mg compared to NIST-610 for both $^{87}\text{Rb}/^{87}\text{Sr}$ and $^{86}\text{Sr}/^{87}\text{Sr}$ ratios (Fig. 5). For example,
323 in analytical session 1, the obtained uncertainties for individual $^{87}\text{Rb}/^{87}\text{Sr}$ ratios for the Entire
324 Creek biotite sample are more than double when using Mica-Mg compared to NIST-610 as the
325 PRM (Fig. 5). As a result, the choice of Mica-Mg instead of NIST-610 as the PRM will increase
326 the uncertainties on each analysis, and might consequently mask the presence of multiple data
327 populations. It will also introduces excessive uncertainties onto the calculated isochron dates.

328 The use of Mica-Mg as calibration standard for $^{86}\text{Sr}/^{87}\text{Sr}$ ratios most significantly affects the
329 isochron precision of low-radiogenic samples such as K-feldspar samples. As shown in Table 3
330 and Figure 5, the uncertainty on the K-feldspar isochron dates can be up to $2\times$ larger, compared to
331 other calibration methods. Furthermore, the resulting MSWD values on the isochron regressions
332 are consistently < 0.3 (Table 3), suggesting excessive uncertainties on individual data-points. For

333 the more radiogenic biotite samples, the larger uncertainties in $^{86}\text{Sr}/^{87}\text{Sr}$ ratios have negligible
334 effects to the precision on the isochron dates.

335 The precision of the calibrated $^{87}\text{Rb}/^{87}\text{Sr}$ ratios is more important to the isochron uncertainty of
336 highly radiogenic materials, such as most types of micas. Calibrating to NIST-610 versus Mica-
337 Mg yields either more precise biotite isochron dates or identical precision. However, when NIST-
338 610 is used as the PRM, uncertainty propagation from the MCRM (MDC or Mica-Mg) leads to
339 either identical or slightly worse isochron uncertainties compared to using Mica-Mg as PRM (Fig.
340 5; Table 3). The difference relates to the degree of overdispersion. The larger uncertainties on the
341 Rb/Sr ratios when using Mica-Mg as PRM result in lower MSWD values, reducing the uncertainty
342 on the isochron regression. This excess uncertainty when calibrating to Mica-Mg might mask
343 meaningful geological scatter in Rb/Sr ratios and it is, therefore, advisable to produce isochrons
344 based on data with the best possible analytical precision.

345 In summary, Mica-Mg should not be used as calibration standard for $^{86}\text{Sr}/^{87}\text{Sr}$ ratio calculations
346 for low-radiogenic samples as it introduces excessive uncertainties to age calculations. For high-
347 radiogenic samples, using Mica-Mg as the PRM also introduces larger uncertainties to individual
348 data-points compared to using NIST-610, but there is no significant difference in propagated
349 uncertainty after secondary correction to either MDC or Mica-Mg. For Rb/Sr ratio calibrations,
350 NIST-610 is more consistent, resulting in lower uncertainties on individual Rb/Sr ratios. When
351 there is no overdispersion, this results in better isochron age precision. However, overdispersion
352 can be masked by the increased uncertainties on Rb/Sr ratios, resulting in better apparent precision
353 when data is calibrated to Mica-Mg.

354 **5.2.2. Accuracy comparisons**

355 It has been observed previously that Rb–Sr dates are offset from their expected ages when
356 calibrated to the NIST-610 reference material (e.g. Gorojovsky and Alard, 2020; Wang et al.,
357 2022). In contrast, Mica-Mg seems to better reproduce expected ages, although the significant
358 uncertainties obtained for natural materials in previous studies render appropriate accuracy testing
359 difficult. For example, Wang et al. (2022) compares measured to expected Rb–Sr dates for three
360 samples with known ages. The best achieved uncertainty in their experiment was ~2.6% for one
361 sample, while for the other samples the reported uncertainties are ~5.6 and 6.3 %. Similarly, the
362 accuracy comparisons in Gorojovsky and Alard (2020) use the Monastery phlogopite, with a
363 precision of ~4% when calibrated to Mica-Mg. Both papers report data normalized to NIST-610
364 but do not apply a secondary correction for matrix-dependent fractionation.

365 For the biotites analysed in our study, the fully propagated 95% confidence interval uncertainties
366 ranges between 0.8 and 1.6% when calibrated to Mica-Mg and between 1.0% and 1.4% when
367 calibrated to NIST-610 and corrected to MDC (depending on the sample and analytical session;
368 Table 3), allowing for more detailed accuracy comparisons. Figure 4 illustrates that using NIST-
369 610 and MDC as calibration reference materials produces the most accurate results, compared to
370 the expected references dates. For the biotite results, the obtained Rb–Sr dates are within 0.5%
371 accuracy compared to the expected ages. The K-feldspar dates are accurate within 1%, except for
372 session 2, where accuracy is within 1.5%. When the same data is calibrated against Mica-Mg
373 (either using NIST-610 as the PRM and Mica-Mg as MCRM, or directly using Mica-Mg as the
374 PRM), the results are significantly offset from their expected ages. For the biotite results calibrated
375 to Mica-Mg, accuracy is within 2% for sessions 2 and 3 and there is 5% age off-set in session 1.
376 For the K-feldspars, the age offset is up to 2.5% in sessions 2 and 3 and 6% in session 1. While the

377 age offsets in sessions 2 and 3 might be regarded as 'acceptable', given the obtained precision, the
378 more significant inaccuracy in session 1 renders Mica-Mg to be less desirable as a PRM.
379 The difference in accuracy between session 1 and sessions 2 and 3 can be explained by the
380 difference in measured dates for the MDC and Mica-Mg reference materials, normalised to NIST-
381 610. For sessions 2 and 3, MDC and Mica-Mg produced similar isochron dates (2.3 and 1.9%
382 difference respectively) (Table 3; Fig. 6). For session 1, however, MDC gives a significantly
383 different age (494 ± 4 Ma) compared to Mica-Mg (469 ± 4 Ma). These differences in accuracy (ca.
384 5 % in session 1 and ca. 2 % in sessions 2 and 3) are in line with the observed age off-sets between
385 the measured dates and reference dates for the biotite and K-feldspar samples, calibrated to Mica-
386 Mg.

387

388 **5.2.3. Long-term comparison between MDC and Mica-Mg as secondary calibration** 389 **standards**

390 Given that the accuracy of the Rb–Sr method appears to be significantly dependent on the applied
391 calibration reference materials, and that the measured Rb–Sr dates of these calibration standards
392 fluctuate significantly between analytical sessions when compared to NIST-610, the long-term
393 behaviour of the MDC and Mica-Mg reference materials needs to be evaluated. Figure 7 presents
394 2.5 years of measured Rb–Sr dates for MDC and Mica-Mg, both calibrated to NIST-610 as the
395 PRM. All data in this plot have been processed identically. The Rb–Sr dates for Mica-Mg are
396 generally more consistent, ranging between ca. 462 and 479 Ma, with a standard deviation of 4.5
397 Ma, while the MDC dates show more variation, ranging between ca. 465 and 494 Ma, with a
398 standard deviation of 7.7 Ma. In all but two sessions, MDC produces an older Rb–Sr date compared
399 to Mica-Mg. The analytical sessions discussed above are highlighted in Figure F and encompass

400 the maximum variability in measured Rb–Sr dates for MDC. With the premise that calibration to
401 NIST-610 and MDC produces accurate Rb–Sr dates (as discussed in section 5.2.2), the difference
402 between the measured MDC and Mica-Mg dates (Fig. 6, 7) can be regarded as an estimate of the
403 degree of inaccuracy when data is calibrated to Mica-Mg. While some sessions reveal very little
404 off-set between both standards, using Mica-Mg as calibration standard can lead to up to 5%
405 inaccuracy in Rb–Sr dates. The cause of the observed variability is currently unknown, however,
406 in the second-to-last session with a significantly older Mica-Mg date compared to MDC, the
407 analysed samples might have received a lower effective laser fluence compared to other sessions
408 as the glass between the laser beam and samples was not cleaned prior to analysis. The lower
409 fluence could change the effective matrix bias between NIST-610, Mica-Mg and MDC, however,
410 calibration of biotite against MDC produces accurate results as demonstrated in section 5.2.2. In
411 contrast, although Mica-Mg produces more consistent Rb–Sr dates between analytical sessions,
412 these dates are unreliable given the variable and unsystematic degree of inaccuracy between
413 sessions.

414

415 **6. Conclusions**

416 Based on our observations, the use of Mica-Mg as calibration reference material is not
417 recommended, for the following reasons:

- 418 (1) The down-hole fractionation (DHF) trend for Mica-Mg is not comparable with the DHF
419 trends of natural biotite, phlogopite and K-feldspar (Fig. 1). Using Mica-Mg to correct DHF
420 would exacerbate instead of reduce DHF in those minerals;

421 (2) Given the relatively poor reproducibility of $^{87}\text{Rb}/^{87}\text{Sr}$ ratios and significant uncertainty on
422 individual $^{87}\text{Sr}/^{86}\text{Sr}$ measurements (Fig. 2), Mica-Mg as PRM or MCRM introduces excess
423 uncertainty that can be avoided using a more consistent PRM such as NIST-610;

424 (3) We demonstrated that calibrating to Mica-Mg may lead to up to 5% inaccuracy in Rb–Sr
425 age (Fig. 4, 6, 7) and that the degree of inaccuracy is unsystematically session-dependant.

426 We suggest a different approach, involving (1) calibration of the $^{87}\text{Rb}/^{87}\text{Sr}$ and $^{87}\text{Sr}/^{86}\text{Sr}$ ratios to a
427 primary reference material with high Rb and Sr concentrations and homogenous isotopic ratios
428 such as NIST-610 glass, including DHF correction of the Rb/Sr ratios, followed by (2) a correction
429 of the $^{87}\text{Rb}/^{87}\text{Sr}$ ratio to a natural mineral MCRM with a similar DHF trend as the samples to be
430 analysed. In our observations with a $67\mu\text{m}$ spot-size, there are no significant differences in matrix
431 effects comparing biotite, phlogopite and K-feldspar, suggesting that any of these natural minerals
432 as MCRM can produce accurate dates for K-rich minerals. We have used MDC phlogopite as
433 MCRM and demonstrate accurate Rb–Sr dates for a range of biotites and K-feldspars with well-
434 established age constraints. For the biotite dates, the fully propagated uncertainties for the analysed
435 biotites are $<1.5\%$, allowing accuracy verifications at high analytical precision. The K-feldspar
436 dates have relative high uncertainties (ca. 5-10%) and, therefore, the accuracy of the calibration
437 cannot robustly be tested. However, absolute values agree with biotite dates and for a given sample,
438 biotite and K-feldspar analyses statistically constitute a single isochron.

439 Finally, while this two-step calibration protocol is currently recommended due to current
440 constraints with data processing software, new developments involving calibrating to isochronous
441 reference materials might become the desired approach in the future.

442

443 **Data availability**

444 The Rb–Sr dataset used in this manuscript is freely available on figshare at
445 <https://doi.org/10.25909/23996484>.

446

447

448 **Acknowledgements**

449 This paper was supported by research grant FT210100906 and DP220103037 from the Australian
450 Research Council (ARC).

451

452

453 **Author contributions**

454 SG: Conceptualization, investigation, writing – original draft, methodology, funding acquisition,
455 visualisation, formal analysis

456 SEG: Conceptualization, investigation, writing – review and editing, methodology

457 MH: Conceptualization, investigation, writing - review and editing, resources

458 JCL: Conceptualization, investigation, writing - review and editing, formal analysis

459

460 **Competing interests**

461 The authors declare that they have no conflict of interest.

462

463 **Ethical statement**

464 This manuscript is an original work that is not submitted or published elsewhere.

465

	React. gas (ml.min ⁻¹)	Laser wavel. (nm)	Fluence (J.cm ⁻²)	Rep. rate (Hz)	Spot (μm)	Rb-Sr calibration	Sr-Sr calibration	DHF	Err. corr.
Zack and Hogmalm 2016	O ₂ (0.25)	213	7	10	80	Pl: NIST-610; Ksp: BCR-2G; Bt: La Posta	NIST-610	No	No
Hogmalm et al. 2017	O ₂ (0.25) N ₂ O (0.16) SF ₆ (0.04)	213	O ₂ : 7 N ₂ O: 6-8 SF ₆ : 6-8	10 4-5 10	80 50 50	Mica-Mg	NIST-610	No	No
Tillberg et al. 2020	N ₂ O (?)	213	?	?	50	BCR-2G (Sec: Mica- Mg/La Posta)	NIST-610	No	Yes
Rösel and Zack 2022	N ₂ O (0.18- 0.20)	213	5-7	10	50- 60	Mica-Mg (sec: NIST- 610 / BCR-2G)	Mica-Mg	No	No
Gorojovsky and Alard 2020	N ₂ O (0.25)	193 and 213	7.8	5	85	Mica-Mg	Mica-Mg, NIST-610, BHVO-2G	No	No?
Larson et al 2023	N ₂ O (0.37)	193	4	10	50	Mica-Mg (Sec: Mica-Fe)	NIST-610	Yes?	Yes
Laureijs et al. 2021	CH ₃ F (10%)	213	6	10	50	ATHO-G, T1- G, StHs6/80-G	NIST-612	No	Yes
Li et al. 2020	N ₂ O (0.35)	193	3.5	5	74	Mica-Mg Sec: MDC	Mica-Mg	No	No
Liebmann et al. 2022	N ₂ O (?)	193	2.5	5	64	NIST-610 + Mica-Mg Sec: CK001 bt	NIST-610	No	Yes
Olierook et al. 2020	N ₂ O (0.25)	193	2.5	5	64- 87	NIST-610 + Mica-Mg Sec: CK001 bt	NIST-610	No	No
Redaa et al. 2021	N ₂ O (0.37)	193	3.5	5	74	Mica-Mg Sec: MDC	Mica-Mg	mon itore d	No
Sengun et al. 2019	N ₂ O (?)	213	5.7	10	50	Mica-Mg	NIST-610	No	No
Tilberg et al. 2021	N ₂ O (?)	213	?	?	50	Mica-Mg / NIST 610	NIST-610	No	Yes
Wang et al. 2022	N ₂ O (0.25)	193	7	5	85	Mica-Mg	NIST-610, BHVO- 2G, BCR-2G	mon itore d	No
Kirkland et al. 2023	N ₂ O (0.25)	193	2	5	64	Mica-Mg Sec: CK001 bt	NIST-610	No	No

467 **Table 1:** Summary of published analytical conditions and protocols for LA-ICP-MS/MS Rb–Sr
468 dating. Rep. rate = laser repetition rate; Sec = secondary reference material; Bt = biotite; ksp = K-
469 feldspar; Pl = plagioclase; Err. Corr. = error correlation calculated (in most cases based on
470 calculated uncertainties after data-reduction rather than during data-reduction); In case of method
471 development work - `best conditions` are quoted.

472

Analytical conditions

Plasma Settings	
RF power	1350 W
Sample Depth	5.0 mm
Ar carrier gas	0.89 L/min
He carrier gas	0.38 L/min
N ₂ addition	4 mL/min
Lens Parameters	
Extract 1	1.5 V
Extract 2	-80 V
Omega Bias	-85 V
Omega Lens	5.0 V
Q1 entrance	-10 V
Q1 exit	-2.0 V
Cell focus	-2.0 V
Cell Entrance	-90 V
Cell Exit	-120 V
Deflect	10 V
Plate Bias	-80 V
Q1 bias	-2.0 V
Q1 Prefilter Bias	-10.0 V
Q1 Postfilter Bias	-10.0 V
N ₂ O gas flow	0.37 mL/min
Octopole bias	-6.0 V
Axial Acceleration	2.0 V
Octopole RF	180 V
Energy Discrimination	-7.0 V
Analysis Parameters	
Laser Wavelength	193 nm
Laser fluence	3.5 J/m ²
Sample laser diameter	67 μm
Laser repetition rate	5 Hz
Background	30 s
Analysis time	40 s
Isotopes measured & dwell times (ms)	²³ Na (2), ²⁴ Mg (2), ²⁷ Al (2), ²⁹⁺¹⁶ Si (2), ³¹⁺¹⁶ P (2), ³⁹ K (2), ⁴³⁺¹⁶ Ca (2), ⁵⁵ Mn (2), ⁵⁶⁺¹⁶ Fe (2), ⁸⁵ Rb (10), ⁸⁶⁺¹⁶ Sr (50), ⁸⁷⁺¹⁶ Sr (50), ⁸⁸⁺¹⁶ Sr (50), ⁸⁹⁺¹⁶ Y (5), ⁹⁰⁺³² Zr (5), ⁹³⁺³² Nb (5), all x+16REE (5), ²³²⁺¹⁵ Th (5), ²³⁸⁺¹⁶ U (5)

473

474

475 **Table 2:** Analytical conditions for the three LA-ICP-MS/MS sessions in this paper.

Sample (exp. age)	S	n	(A) NIST-610 + MDC		(B) NIST610 + Mica-Mg		(C) Mica-Mg & NIST-610		(D) Mica-Mg	
			Age ($\pm 2\sigma$) [Ma]	MS WD	Age ($\pm 2\sigma$) [Ma]	MS WD	Age ($\pm 2\sigma$) [Ma]	MS WD	Age ($\pm 2\sigma$) [Ma]	MS WD
Ent Crk Bt (312.1 \pm 1.8 ¹)	1	24	310.7 \pm 1.5/2.5/3.1	1.1	327.8 \pm 1.7/2.7/3.2	0.96	327.6 \pm 3.3/3.9	0.27	328.8 \pm 3.4/4.0	0.25
	3	20	311.6 \pm 3.1/3.8/4.5	2.5	317.6 \pm 3.2/3.8/4.6	2.4	316.1 \pm 3.2/3.8	0.85	316.2 \pm 3.2/3.8	0.84
Bund1b Bt (286.2 \pm 2.2 ²)	2	44	287.1 \pm 1.6/2.4/3.4	1.6	280.3 \pm 1.5/2.4/3.2	1.7	280.1 \pm 1.6/2.4	0.97	280.2 \pm 1.6/2.4	0.82
	3	22	284.7 \pm 2.4/3.0/3.8	1.0	290.1 \pm 2.5/3.1/3.8	1.1	288.4 \pm 4.1/4.5	0.7	288.2 \pm 4.3/4.7	0.28
Bund1b Ksp (286.2 \pm 2.2 ²)	2	57	290 \pm 14/14/14	0.87	284 \pm 14/14/14	0.88	284 \pm 14/14	0.84	280 \pm 23/23	0.3
	3	53	287 \pm 15/15/15	0.88	292 \pm 15/15/15	0.88	290 \pm 15/16	0.86	283.4 \pm 38/38	0.19
Bund6a Bt (286.2 \pm 2.2 ²)	2	38	287.7 \pm 1.3/2.3/3.4	1.4	280.9 \pm 1.3/2.2/3.1	1.5	279.5 \pm 1.5/2.3	0.71	279.5 \pm 1.5/2.3	0.7
	3	22	285.7 \pm 1.9/2.6/3.4	0.74	291.2 \pm 1.9/2.7/3.6	0.72	288.7 \pm 3.5/4.0	0.54	288.8 \pm 3.6/4.0	0.34
Bund6a Ksp (286.2 \pm 2.2 ²)	2	45	290 \pm 37/37/37	0.69	283 \pm 36/36/36	0.69	281 \pm 36/36	0.68	283 \pm 75/75	0.16
	3	40	288 \pm 37/37/37	0.65	293 \pm 38/38/38	0.65	294 \pm 39/39	0.65	296 \pm 93/93	0.11
Taratap Bt (497.1 \pm 0.6 ³)	2	30	499.4 \pm 1.8/3.6/5.6	1.2	487.7 \pm 1.7/3.5/5.2	1.2	489.6 \pm 2.8/4.2	0.67	489.6 \pm 2.8/4.2	0.63
	3	16	495.7 \pm 2.5/4.0/5.5	1.2	505.1 \pm 2.6/4.1/5.8	1.2	504.0 \pm 5.4/6.3	0.51	504.0 \pm 5.5/6.3	0.52
Taratap Ksp (497.1 \pm 0.6 ³)	1	54	500 \pm 30/30/30	0.53	527 \pm 31/31/31	0.53	527 \pm 32/32	0.50	539 \pm 58/58	0.14
	2	20	501 \pm 50/50/50	0.58	490 \pm 49/49/49	0.58	492 \pm 50/50	0.56	494 \pm 106/106	0.12
	3	18	495 \pm 35/35/35	0.95	504 \pm 36/36/36	0.95	490 \pm 39/39	1.1	511 \pm 63	0.3

476

477

MCRM	S	n	NIST-610 as PRM	
			Age ($\pm 2\sigma$) [Ma]	MS WD
MDC	1	34	494.4 \pm 3.0	1.4
	2	21	464.5 \pm 4.0	1.3
	3	30	470.6 \pm 3.6	1.1
Mica-Mg	1	35	468.6 \pm 2.5	2.8
	2	21	475.7 \pm 3.7	3.5
	3	20	461.8 \pm 3.7	2.7

478

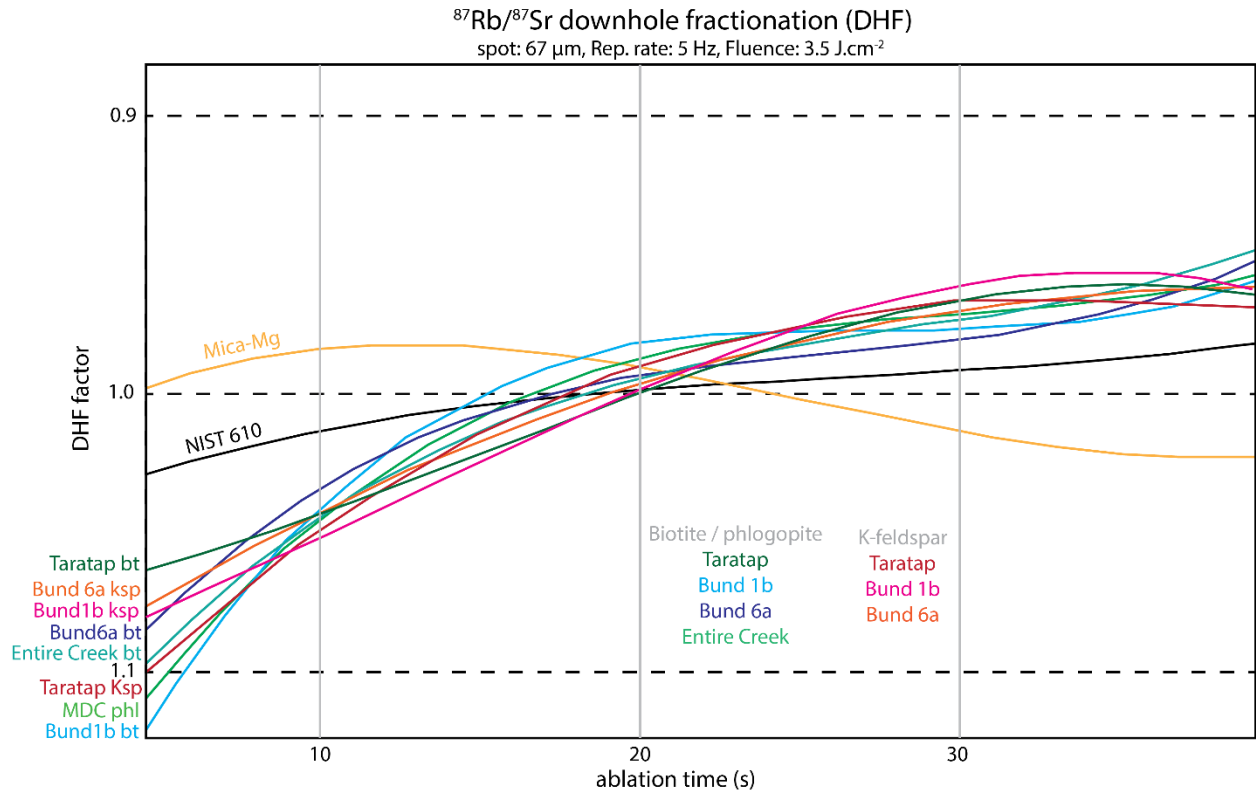
479

480 **Table 3:** Summary table of Rb–Sr dates obtained in this study. S = session number, n = number of analysed grains, exp. age = expected
481 reference age (see below). All uncertainties are 95% confidence intervals and are reported as (1) excluding external uncertainty (on the
482 decay constant) / (2) including external uncertainties / (3) with propagated uncertainty from the correction standard (for methods (A)
483 and (B) only). (A) NIST-610 as PRM and MDC as MCRM to calibrate Rb/Sr ratios; (B) NIST-610 as PRM, Mica-Mg as MCRM to
484 calibrate Rb/Sr ratios; (C) Rb/Sr ratios calibrated to Mica-Mg as PRM and Sr/Sr ratios calibrated to NIST-610 as PRM; (D) Mica-MG
485 as PRM for both Rb/Sr and Sr/Sr ratios. ¹ Rb-Sr TIMS age from Mortimer et al. (1987), recalculated with Villa et al. (2015) decay
486 constant in IsoplotR (Vermeesch, 2018). The reported uncertainty is 95% confidence interval but does not take overdispersion into
487 account. ² Zircon U-Pb age for the Banalasta Adamellite in the Bundarra Suite, from Black (2007). ³ Zircon U-Pb TIMS age for the
488 Taratap Granodiorite, reported in Glorie et al. (2023).

489

490 **Figure Captions**

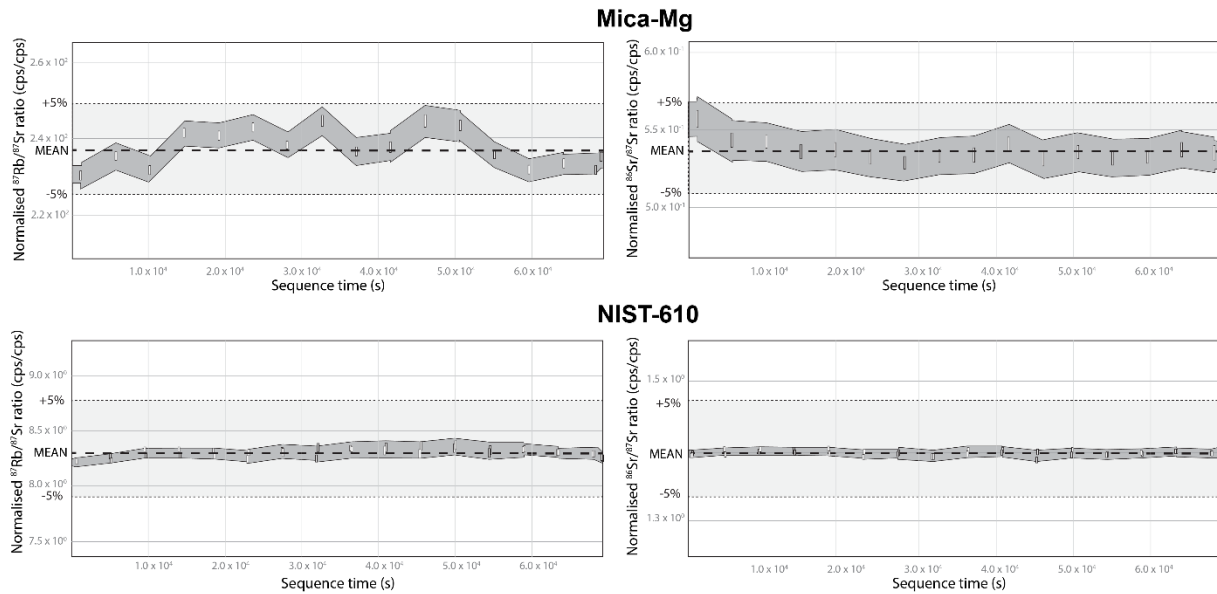
491



492

493 **Figure 1:** ⁸⁷Rb/⁸⁷Sr downhole fractionation profiles for the analysed reference materials Mica-Mg
494 (yellow line) and NIST-610 (black line), the biotite / phlogopite (green-blue lines) and K-feldspar
495 (red-pink lines) samples in analytical session 3, calculated in LADR (Norris and Danyushevsky,
496 2018). The DHF factor is calculated relative to the average ratio of the ablation signal (i.e. DHF
497 factor of 1 = average ⁸⁷Rb/⁸⁷Sr ratio of the downhole signal).

498



499

500 **Figure 2:** Variability of the $^{87}\text{Rb}/^{87}\text{Sr}$ and $^{86}\text{Sr}/^{87}\text{Sr}$ ratios for the analysed reference materials

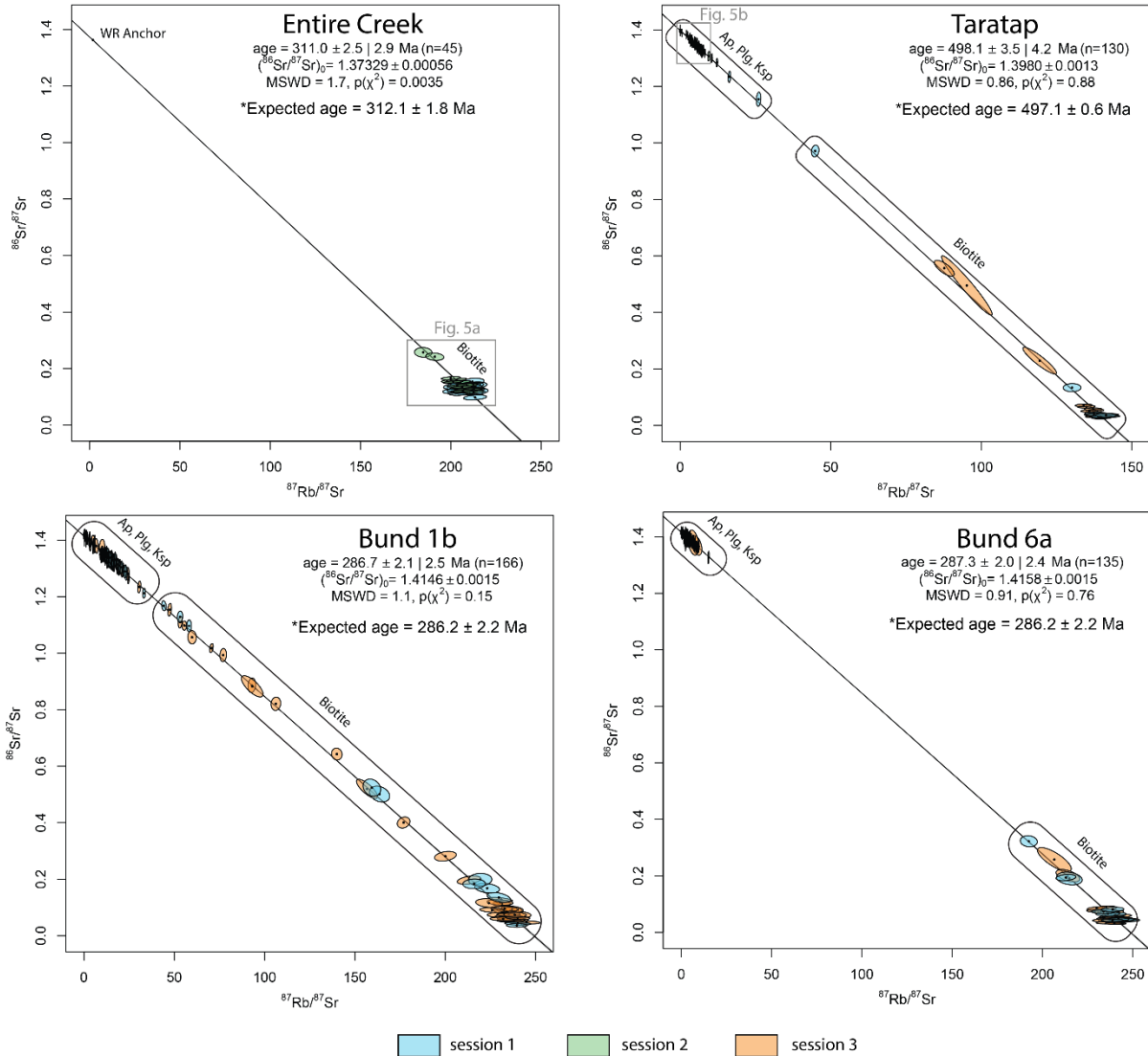
501 NIST-610 and Mica-Mg over the total duration of analytical session 3 (prior to drift correction).

502 All plots are scaled equally to $\pm 5\%$ variation of the mean to aid visual comparisons. The vertical

503 bars are ± 1 standard deviation. The gray envelopes models ± 2 standard deviation (note that for

504 NIST-610 each standard was measured twice at each standard bracket).

505



506

507 **Figure 3:** Pooled multi-mineral Rb–Sr isochron dates for the Entire Creek, Taratap and the two

508 Bundarra samples (Bund 1b and Bund 6a). The data was calibrated against NIST-610 as PRM and

509 MDC as MCRM (see text for details). The colour-code refers to the analytical session in which

510 the data was obtained. Biotite analyses plot towards the radiogenic lower-intercept of the inverse

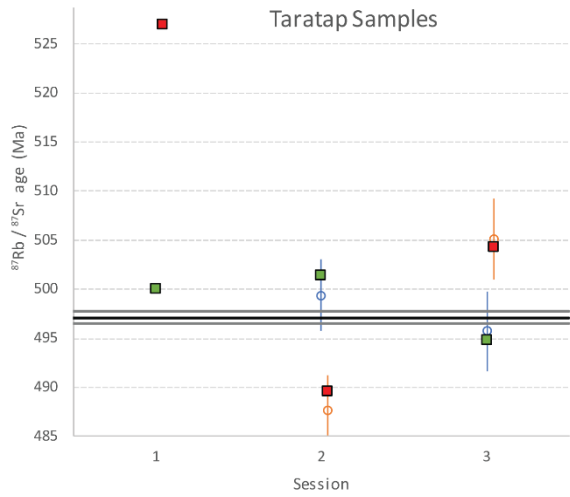
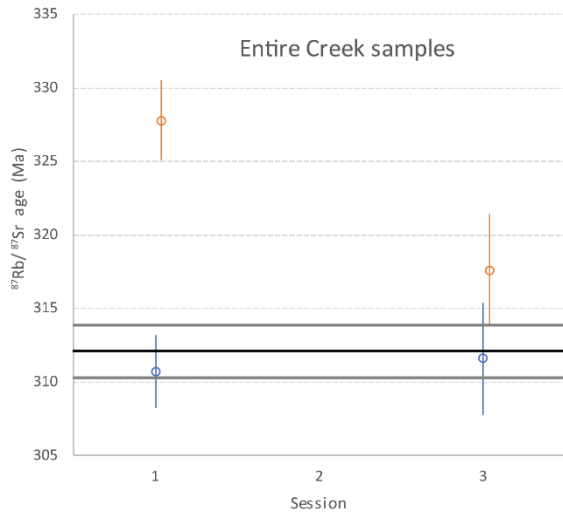
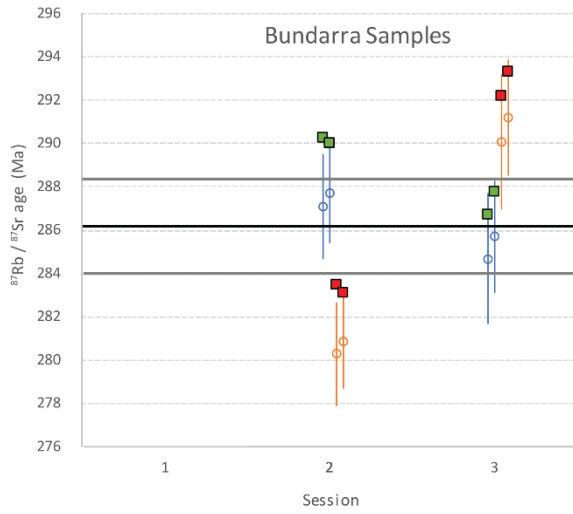
511 isochrons, while feldspar and apatite anchor Rb/Sr ratios plot towards the low-radiogenic end of

512 the isochron regression. All plots were calculated in IsoplotR (Vermeesch, 2018), reporting 95%

513 confidence interval uncertainties (including the uncertainty on the decay-constant) with and

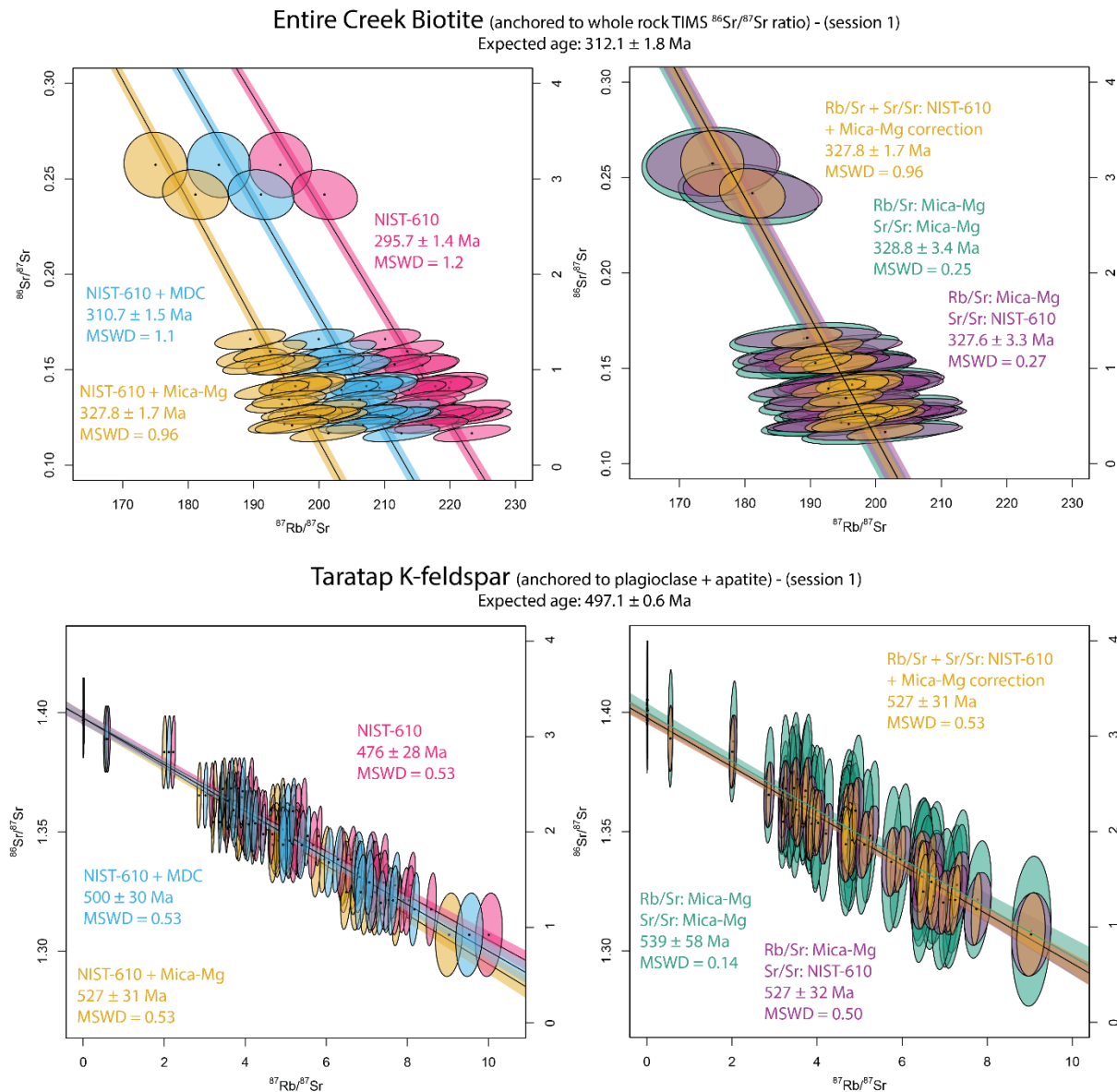
514 without propagated uncertainty from the MDC MCRM. Expected ages are the recalculated Rb–Sr

515 age from Mortimer et al. (1987) with the Villa et al. (2015) decay constant for the Entire Creek
516 sample; the zircon U-Pb ID-TIMS age reported in Glorie et al. (2023) for the Taratap sample, and
517 the Zircon SHRIMP U-Pb age from Black (2007) for the Bundarra samples (see text for further
518 details).
519



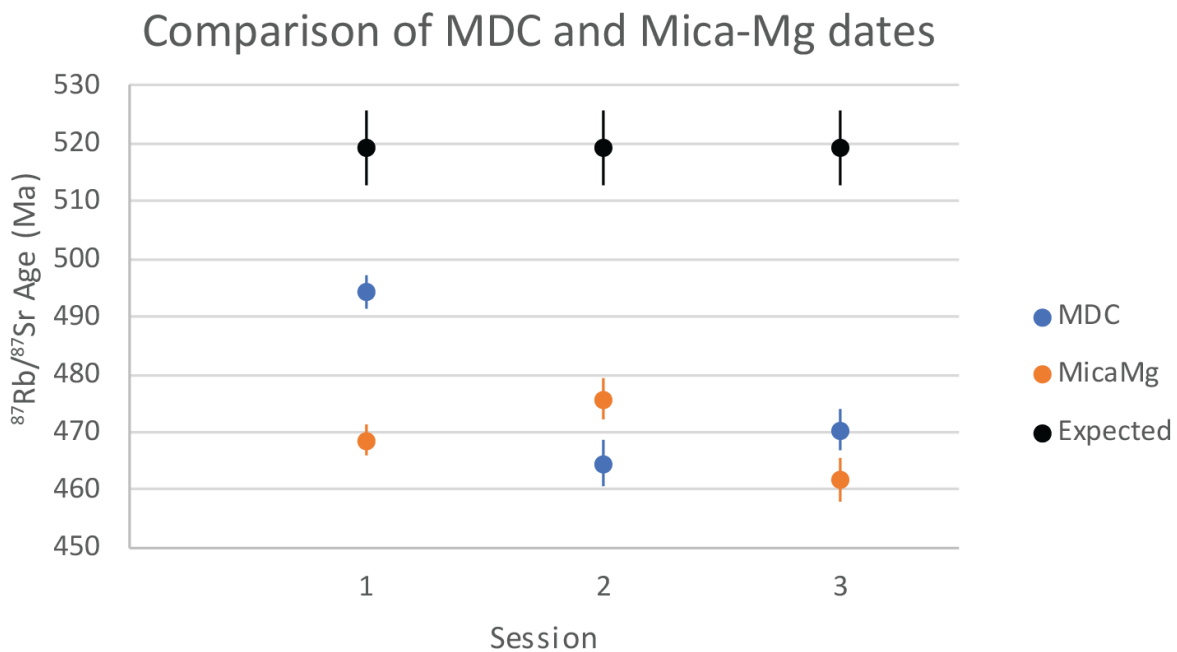
521 **Figure 4:** Comparisons of Rb–Sr dates over three analytical sessions, calibrated to either MDC or
 522 Mica-Mg as MCRM, with respect to the expected ages for each sample (black line with gray 2SE
 523 uncertainty bars). In all cases, NIST-610 was used as PRM. Biotite data are plotted as open circles
 524 (blue = calibrated to MDC as MCRM, orange = calibrated to Mica-Mg as MCRM). K-feldspar
 525 data are plotted as filled squares (green = calibrated to MDC as MCRM, red = calibrated to Mica-
 526 Mg as MCRM).

527



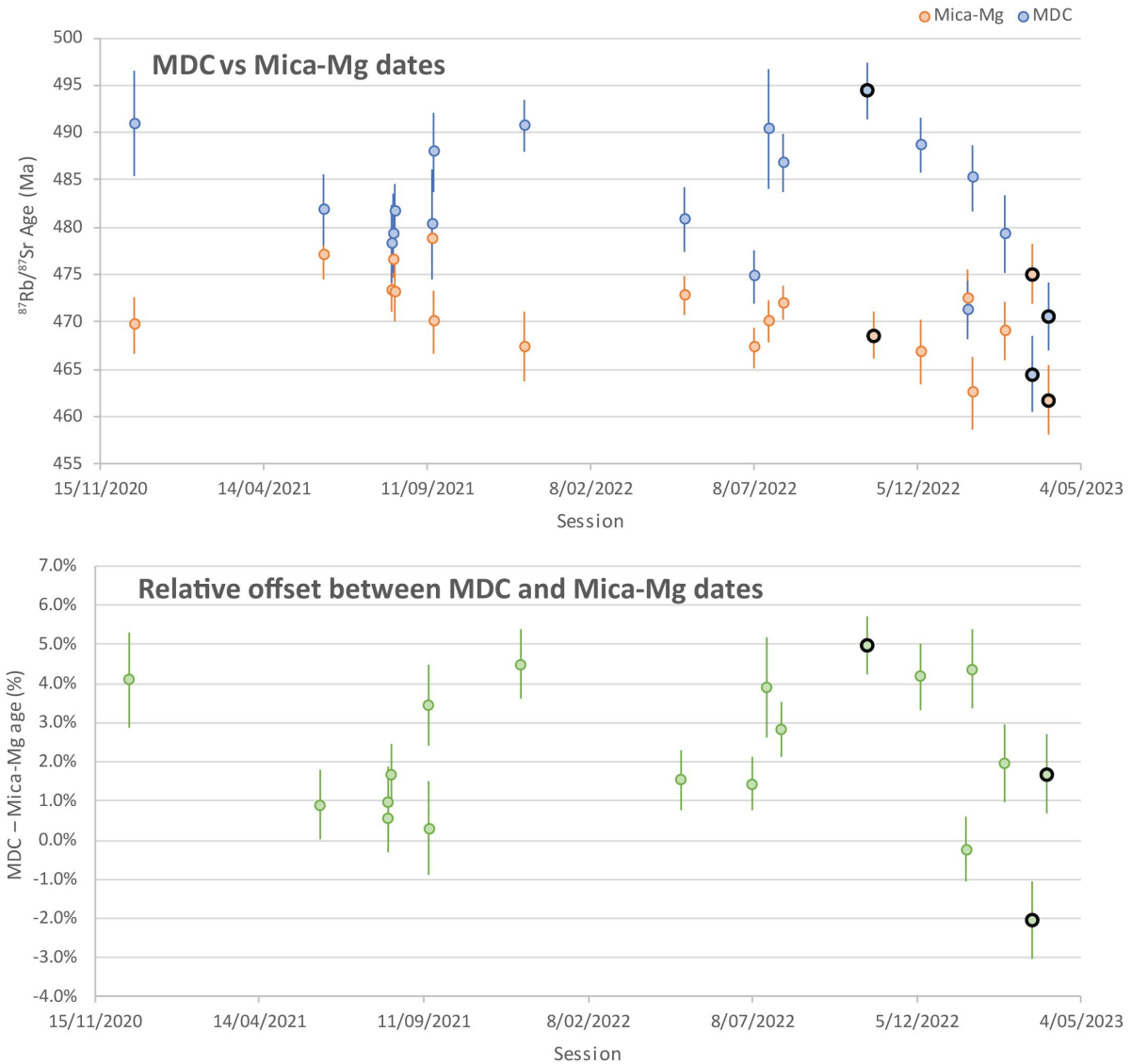
528

529 **Figure 5:** Comparisons of isochron dates obtained using the 4 different calibration protocols using
 530 the session 1 biotite Rb–Sr data from the Entire Creek sample and K-feldspar Rb–Sr data from the
 531 Taratap sample. Data plotted in red = NIST-610 as PRM without correction for matrix-induced
 532 fractionation. Data plotted in green = NIST-610 as PRM with Mica-Mg as MCRM. Data plotted
 533 in yellow = NIST-610 as PRM with MDC as MCRM. Data plotted in purple = NIST-610 as PRM
 534 for Sr/Sr ratios and Mica-Mg as PRM for Rb/Sr ratios. Data plotted in blue = both Rb/Sr and Sr/Sr
 535 ratios calibrated to Mica-Mg as PRM. The biotite data are highly radiogenic and show significant
 536 age differences depending on the used MCRM. The K-feldspar data are low radiogenic, resulting
 537 in larger and overlapping uncertainties (refer to Figure 3 for full isochron plots). Using NIST-610
 538 as PRM produces the smallest uncertainties on individual data-points.
 539



540

541 **Figure 6:** Rb–Sr dates for MDC and Mica-Mg calibrated to NIST-610 over the three analytical
 542 sessions used in this paper. The off-set of the Rb–Sr age with respect to the reference age is used
 543 to calculate the correction factor on the Rb/Sr ratios. Uncertainties are 2SE.
 544



545
 546 **Figure 7:** Long-term (2.5 years) Rb–Sr age data for Mica-Mg and MDC for the lab (Adelaide
 547 Microscopy). All uncertainties are 2SE. The top plot shows absolute dates and the bottom plot
 548 shows the percentage difference between the MDC and Mica-Mg dates. All data were processed

549 in the same way using NIST-610 as PRM. The three analytical sessions previously discussed are
550 highlighted by black rims and capture the most extreme differences obtained in our lab to date.
551 Given that MDC as MCRM produces consistently accurate data, the plot indicates that Mica-Mg
552 as PRM can lead to up to 5% inaccuracy in Rb–Sr age calculations.

553

554 **References**

- 555 Balcaen, L., Bolea-Fernandez, E., Resano, M., Vanhaecke, F., 2015. Inductively coupled plasma – Tandem
556 mass spectrometry (ICP-MS/MS): A powerful and universal tool for the interference-free
557 determination of (ultra)trace elements – A tutorial review. *Analytica Chimica Acta*, 894: 7-19.
- 558 Black, L., 2007. SHRIMP U–Pb zircon ages obtained during 2006/07 for NSW Geological Survey projects.
- 559 Burt, A.C., Abbot, P.J., 1998. The Taratap Granodiorite, South-East South Australia. *MESA Journal*, 10:
560 35-39.
- 561 Flood, R.H., Shaw, S.E., 1975. A cordierite-bearing granite suite from the New England Batholith, N.S.W.,
562 Australia. *Contributions to Mineralogy and Petrology*, 52(3): 157-164.
- 563 Flood, R.H., Shaw, S.E., 1977. Two “S-type” granite suites with low initial $^{87}\text{Sr}/^{86}\text{Sr}$ ratios from the New
564 England Batholith, Australia. *Contributions to Mineralogy and Petrology*, 61(2): 163-173.
- 565 Glorie, S. et al., 2023. Robust laser ablation Lu-Hf dating of apatite: an empirical evaluation. *Geological*
566 *Society of London Special Publication*, In press.
- 567 Gorojovsky, L., Alard, O., 2020. Optimisation of laser and mass spectrometer parameters for their
568 situ analysis of Rb/Sr ratios by LA-ICP-MS/MS. *JOURNAL OF ANALYTICAL ATOMIC SPECTROMETRY*,
569 35(10): 2322-2336.
- 570 Hogmalm, K.J., Zack, T., Karlsson, A.K.O., Sjöqvist, A.S.L., Garbe-Schonberg, D., 2017. In situ Rb-Sr and K-
571 Ca dating by LA-ICP-MS/MS: an evaluation of N₂O and SF₆ as reaction gases. *Journal of Analytical*
572 *Atomic Spectrometry*, 32(2): 305-313.
- 573 Jackson, S.E., Günther, D., 2003. The nature and sources of laser induced isotopic fractionation in laser
574 ablation-multicollector-inductively coupled plasma-mass spectrometry. *Journal of Analytical*
575 *Atomic Spectrometry*, 18(3): 205-212.
- 576 Jegal, Y. et al., 2022. Characterisation of Reference Materials for In Situ Rb-Sr Dating by LA-ICP-MS/MS.
577 *Geostandards and Geoanalytical Research*, 46(4): 645-671.
- 578 Jeon, H., Williams, I.S., Chappell, B.W., 2012. Magma to mud to magma: Rapid crustal recycling by Permian
579 granite magmatism near the eastern Gondwana margin. *Earth and Planetary Science Letters*, 319-
580 320: 104-117.
- 581 Kirkland, C.L. et al., 2023. Dating mylonitic overprinting of ancient rocks. *Communications Earth &*
582 *Environment*, 4(1): 47.
- 583 Košler, J. et al., 2005. Chemical and phase composition of particles produced by laser ablation of silicate
584 glass and zircon—implications for elemental fractionation during ICP-MS analysis. *Journal of*
585 *Analytical Atomic Spectrometry*, 20(5): 402-409.
- 586 Larson, K.P., Button, M., Shrestha, S., Camacho, A., 2023. A comparison of $^{87}\text{Rb}/^{87}\text{Sr}$ and $^{40}\text{Ar}/^{39}\text{Ar}$
587 dates: Evaluating the problem of excess ^{40}Ar in Himalayan mica. *Earth and Planetary Science*
588 *Letters*, 609: 118058.

589 Laureijs, C.T., Coogan, L.A., Spence, J., 2021. In-situ Rb-Sr dating of celadonite from altered upper oceanic
590 crust using laser ablation ICP-MS/MS. *Chemical Geology*, 579.

591 Li, S.-S. et al., 2020. Coupled U-Pb and Rb-Sr laser ablation geochronology trace Archean to Proterozoic
592 crustal evolution in the Dharwar Craton, India. *Precambrian Research*, 343: 105709.

593 Li, Y., Vermeesch, P., 2021. Short communication: Inverse isochron regression for Re-Os, K-Ca and other
594 chronometers. *Geochronology*, 3(2): 415-420.

595 Liebmann, J., Kirkland, C.L., Kelsey, D.E., Korhonen, F.J., Rankenburg, K., 2022. Lithological fabric as a proxy
596 for Rb-Sr isotopic complexity. *Chemical Geology*, 608.

597 Longerich, H.P., Günther, D., Jackson, S.E., 1996. Elemental fractionation in laser ablation inductively
598 coupled plasma mass spectrometry. *Fresenius' Journal of Analytical Chemistry*, 355(5): 538-542.

599 Moens, L.J., Vanhaecke, F.F., Bandura, D.R., Baranov, V.I., Tanner, S.D., 2001. Elimination of isobaric
600 interferences in ICP-MS, using ion-molecule reaction chemistry: Rb/Sr age determination of
601 magmatic rocks, a case study. *Journal of Analytical Atomic Spectrometry*, 16(9): 991-994.

602 Mortimer, G.E., Cooper, J.A., James, P.R., 1987. U-Pb and Rb-Sr geochronology and geological
603 evolution of the Harts Range ruby mine area of the Arunta Inlier, central Australia. *Lithos*, 20(6):
604 445-467.

605 Norris, A., Danyushevsky, L., 2018. Towards Estimating the Complete Uncertainty Budget of Quantified
606 Results Measured By LA-ICP-MS. *Goldschmidt, Boston, USA (2018)*.

607 Olierook, H.K.H. et al., 2020. Resolving multiple geological events using in situ Rb-Sr geochronology:
608 implications for metallogenesis at Tropicana, Western Australia. *Geochronology*, 2(2): 283-303.

609 Phillips, G., Landenberger, B., Belousova, E.A., 2011. Building the New England Batholith, eastern
610 Australia—Linking granite petrogenesis with geodynamic setting using Hf isotopes in zircon.
611 *Lithos*, 122(1): 1-12.

612 Redaa, A. et al., 2023. Testing Nano-Powder and Fused-Glass Mineral Reference Materials for In Situ Rb-
613 Sr Dating of Glauconite, Phlogopite, Biotite and Feldspar via LA-ICP-MS/MS. *Geostandards and
614 Geoanalytical Research*, 47(1): 23-48.

615 Redaa, A. et al., 2021. Assessment of elemental fractionation and matrix effects during in situ Rb-Sr dating
616 of phlogopite by LA-ICP-MS/MS: implications for the accuracy and precision of mineral ages.
617 *Journal of Analytical Atomic Spectrometry*, 36(2): 322-344.

618 Roberts, N.M.W. et al., 2017. A calcite reference material for LA-ICP-MS U-Pb geochronology.
619 *Geochemistry, Geophysics, Geosystems*, 18(7): 2807-2814.

620 Rosel, D., Zack, T., 2022. LA-ICP-MS/MS Single-Spot Rb-Sr Dating. *Geostandards and Geoanalytical
621 Research*, 46(2): 143-168.

622 Rosenbaum, G., Li, P., Rubatto, D., 2012. The contorted New England Orogen (eastern Australia): New
623 evidence from U-Pb geochronology of early Permian granitoids. *Tectonics*, 31(1).

624 Sengun, F., Erlandsson, V.B., Hogmalm, J., Zack, T., 2019. In situ Rb-Sr dating of K-bearing minerals from
625 the orogenic Akcaabat gold deposit in the Menderes Massif, Western Anatolia, Turkey. *JOURNAL
626 OF ASIAN EARTH SCIENCES*, 185.

627 Shaw, S.E., Flood, R.H., 1981. The New England Batholith, eastern Australia: Geochemical variations in
628 time and space. *Journal of Geophysical Research: Solid Earth*, 86(B11): 10530-10544.

629 Simpson, A. et al., 2022. In situ Lu-Hf geochronology of calcite. *Geochronology*, 4(1): 353-372.

630 Tillberg, M. et al., 2021. Reconstructing craton-scale tectonic events via in situ Rb-Sr geochronology of
631 poly-phased vein mineralization. *Terra Nova*, 33(5): 502-510.

632 Tillberg, M. et al., 2020. In situ Rb-Sr dating of slickenfibres in deep crystalline basement faults. *Scientific
633 Reports*, 10(1).

634 Vermeesch, P., 2018. IsoplotR: A free and open toolbox for geochronology. *Geoscience Frontiers*, 9(5):
635 1479-1493.

- 636 Villa, I.M., De Bièvre, P., Holden, N.E., Renne, P.R., 2015. IUPAC-IUGS recommendation on the half life of
637 ^{87}Rb . *Geochimica et Cosmochimica Acta*, 164: 382-385.
- 638 Wang, C.Y. et al., 2022. Advances in in-situ Rb-Sr dating using LA-ICP-MS/MS: applications to igneous rocks
639 of all ages and to the identification of unrecognized metamorphic events. *Chemical Geology*, 610.
- 640 Woodhead, J.D., Hergt, J.M., 2001. Strontium, Neodymium and Lead Isotope Analyses of NIST Glass
641 Certified Reference Materials: SRM 610, 612, 614. *Geostandards Newsletter*, 25(2-3): 261-266.
- 642 Zack, T., Hogmalm, K.J., 2016. Laser ablation Rb/Sr dating by online chemical separation of Rb and Sr in an
643 oxygen-filled reaction cell. *Chemical Geology*, 437: 120-133.